THE ASTROPHYSICAL JOURNAL, 429:876–889, 1994 July 10

MAGNETOSTATIC STRUCTURES OF THE SOLAR CORONA. I. A MODEL BASED ON THE CAUCHY BOUNDARY VALUE PROBLEM

J. R. HUNDHAUSEN[1] AND B. C. LOW
High Altitude Observatory, National Center for Atmospheric Research,[2] P.O. Box 3000, Boulder, CO 80307-3000
Received 1993 October 12; accepted 1994 January 6

ABSTRACT

A model is presented for the static equilibrium of a magnetized, polytropic atmosphere stratified by uniform gravity and invariant in a Cartesian direction. The profiles of plasma pressure and magnetic shear as functions of the magnetic stream function, which render the governing equation linear, lead to unphysical features if these profiles are applied to the infinite half-space bounded below by a plane. These undesirable features are shown to be removed when these special profiles are localized to a region bounded by a magnetic flux surface, outside of which is an atmosphere in plane-parallel hydrostatic equilibrium with a potential magnetic field. Two families of solutions are constructed by direct solution of the Cauchy boundary value problem for the Laplace equation, one with continuous and the other with discontinuous pressures across this magnetic boundary. Illustrative solutions are analyzed, with applications to long-lived density enhancements and depletions in the solar corona. In particular, the hydromagnetic stability of pressure discontinuities is studied as an example of a general result due to Hu (1988). It is pointed out that the stability of the sharp interface between the prominence cavity and the high-density coronal helmet may be understood in terms of competing effects arising from density stratification and magnetic curvature. The model presented lays the mathematical groundwork for the other papers of the series.

Subject headings: MHD — Sun: corona — Sun: magnetic fields

1. INTRODUCTION

In the course of an 11 year solar cycle, new magnetic fluxes generated in the solar interior make their way into the corona to spawn a rich variety of plasma structures (e.g., Poland 1986; Zirin 1988). Their formation, structural properties, evolution, and eventual disruption are the physical processes in terms of which one hopes to understand the collective phenomena of solar activity. At times of high solar activity, rapid changes down to timescales of less than a second are observed in the active regions, the flare being the prime example (e.g., Dennis 1985; Tandberg-Hanssen & Emslie 1988). Over larger scales, structures in the corona can persist for such long periods of time (days to weeks) that one needs to ask how the forces creating these structures are kept in equilibrium. Notable are the conspicuous helmet streamers in eclipse pictures of the corona (Billings 1966; Newkirk 1967; Sime & Street 1993. These helmet streamers are of course not truly steady objects. They evolve gradually in a quasi-steady manner, often ending in a disruption into a coronal mass ejection (MacQueen 1980; Fisher 1984; Hundhausen 1988, 1994; Kahler 1992). During the quasi-steady phase of its existence, the helmet streamer poses a basic and interesting problem in hydromagnetic equilibrium (Sturrock & Smith 1968; Pneuman 1972; Pneuman & Kopp 1971; Parker 1979; Priest 1982; Low 1990). In this series of papers, we undertake a study of the force balance associated with long-lived coronal objects. We shall proceed in steps, beginning with this paper and leading eventually to the construction of a model of the helmet streamer containing the essential observable features.

We adopt the first approximation that the coronal structure is in static equilibrium among the Lorentz, pressure, and gravitational forces (Dungey 1953; Low 1975; Hundhausen, Hundhausen, & Zweibel 1981; Uchida & Low 1981). This approximation is reasonable in the low corona, where the subsonic solar wind may be neglected. As is well known, the coronal helmet appears bright in scattered white light because it is a region of enhanced coronal material (Newkirk 1967). A reasonable interpretation is that the nearly (electrically) perfectly conducting helmet material is frozen into and held in equilibrium by the tension force of closed magnetic fields arching over a polarity reversal line on the solar surface. Outside of the helmet, the magnetic fields extend to such great coronal heights that they are open into interplanetary space (Parker 1963; Hundhausen 1972, 1977). The solar wind flows out along these open magnetic fields, which come together above the helmet to form the magnetic neutral sheet in the long streamer. At the base of the helmet a low-density cavity is often found, with a quiescent prominence at the lower part of the cavity (Tandberg-Hanssen 1974; Serio et al. 1978). The corona is optically thin. When the viewing angle is favorable, a white-light image of the corona shows both the helmet and the cavity to have sharp boundaries which suggest extreme magnetic gradients (Saito & Hyder 1968; Saito & Tandberg-Hanssen 1973). Although the helmet streamers in reality can be rather complicated in appearance during times of high solar activity, the above three-part structure—high-density helmet, low-density cavity, prominence—is quite basic. The discovery and the study of coronal mass ejections in the past two decades have placed the helmet streamer in a significant role in solar activity: it is the organizing structure of the large-scale quiescent corona and the origin of a majority of mass ejections (Illing & Hundhausen 1986; Hundhausen 1988, 1994; Low 1990). A theory of this aspect of solar activity must begin with a physical understanding of why the helmet streamer has the three-part structure. Of basic interest is the magnetic topology associated with such a structure.

[1] Also Department of Mathematics, Colorado School of Mines.
[2] The National Center for Atmospheric Research is sponsored by the National Science Foundation.

Even with the simplification of geometric symmetry, the nonlinear hydromagnetic equations are generally intractable. As a step toward a more sophisticated model, we study in this paper, and the one to follow, idealized magnetostatic structures with spatially localized electric currents. This model is formulated in § 2, where it is reduced to a Cauchy boundary value problem for a potential function. Various families of solutions are presented in § 3, illustrating density enhancements and depletions trapped in magnetic fields. Our results are summarized and discussed in § 4.

2. THE MATHEMATICAL MODEL

The equations describing the equilibrium of a static, magnetized atmosphere are:

$$\frac{1}{4\pi}(\nabla \times \boldsymbol{B}) \times \boldsymbol{B} - \nabla p - [\rho + m(S)\delta(S)]g\hat{z} = 0 , \quad (1)$$

$$\nabla \cdot \boldsymbol{B} = 0 , \quad (2)$$

where $\boldsymbol{B}$, p, ρ, and g are, respectively, the magnetic field, the pressure, the density, and the gravitational acceleration taken to be uniform in space directed along $-\hat{z}$ in standard Cartesian coordinates. Equation (1) describes the balance among the Lorentz, pressure, and gravitational forces. To prepare for the study of quiescent prominences in the next paper of the series, we have, for completeness, included the gravitational force on a discrete mass distribution m, associated with a Dirac delta function, over some surface S to be interpreted physically as a prominence sheet (Low & Hundhausen 1994). Taking the system to be independent of the coordinate x, write the magnetic field in the standard form

$$\boldsymbol{B} = \left(Q, \frac{\partial A}{\partial z}, -\frac{\partial A}{\partial y}\right), \quad (3)$$

where A is the stream function. This magnetic field is associated with a current density $\boldsymbol{J} = (c/4\pi)\nabla \times \boldsymbol{B}$, c being the speed of light, where

$$\nabla \times \boldsymbol{B} = \left(-\nabla^2 A, \frac{\partial Q}{\partial z}, -\frac{\partial Q}{\partial y}\right). \quad (4)$$

Equation (1) requires Q to be a strict function of A for equilibrium in the x-direction. Equilibrium in the y-z plane is then described by

$$\frac{1}{4\pi}\left(\nabla^2 A + Q\frac{dQ}{dA}\right)\nabla A + \nabla p + [\rho + m(S)\delta(S)]g\hat{z} = 0 . \quad (5)$$

In the following subsections we formulate a model for the magnetostatic atmosphere described by equation (5). This model is based on a number of assumptions to be introduced at different stages as the formulation proceeds. Some of these assumptions are physically motivated, while the others are introduced for mathematical expediency. Our overriding concern will be to render this formidably nonlinear problem tractable, while preserving physical integrity as much as possible. The end product will be a rich family of (particular) analytic solutions to equation (5) that, without incorporating full generality, will nonetheless be shown to exhibit remarkable versatility in representing the physical properties of the system.

2.1. *Plane Prominence Sheet*

Let us set the photosphere to be a rigid plane at some fixed height $z = z_0 > 0$. Assume symmetry about the z-axis. Take the prominence sheet S to be a flat, vertical surface coincident with the interval $z_0 < a < z < b$ on the z-axis. This surface carries a discrete current flowing in the x-direction:

$$\boldsymbol{J}_{\rm prom} = J_{\rm prom}(S)\delta(S)\hat{x} , \quad (6)$$

generating a discrete Lorentz force along $a < z < b$ on the z-axis to balance the weight of the prominence sheet:

$$\frac{1}{c} J_{\rm prom}(S)\{B_y\}_{y=0} = m(S)g . \quad (7)$$

In equation (5), let us take p and ρ to describe the pressure and density, respectively; of the continuous part of the corona, as opposed to the prominence which is treated as a cold discrete sheet. Hence, p and ρ are smooth functions of space. The weight of the prominence sheet, represented by the term with the delta function, must therefore be balanced by the Lorentz force represented by the term in ∇A. To account for this particular aspect of the balance of forces in equation (5) for the system symmetric about the z-axis, we rewrite equation (7) as follows:

$$m(S)\delta(S)g\hat{z} = \frac{1}{c}\boldsymbol{J}_{\rm prom} \times \boldsymbol{B} = \frac{1}{c} J_{\rm prom}(S)\delta(S)\nabla A , \quad (8)$$

noting that $\partial A/\partial y = 0$ on the z-axis, by symmetry. Equation (5) then takes the form

$$\left[\frac{1}{4\pi}\left(\nabla^2 A + Q\frac{dQ}{dA}\right) + \frac{\partial p(A, z)}{\partial A} + \frac{1}{c} J_{\rm prom}(S)\delta(S)\right]\nabla A + \left(\frac{\partial p(A, z)}{\partial z} + \rho g\right)\hat{z} = 0 , \quad (9)$$

where we have expressed the pressure p in terms of A and z as independent variables. The vectors ∇A and $\hat{z}$ are, in general, independent, and it follows that the forces in the directions of these two vectors must vanish separately:

$$\nabla^2 A + Q\frac{dQ}{dA} + 4\pi\frac{\partial p(A, z)}{\partial A} + \frac{4\pi}{c} J_{\rm prom}(S)\delta(S) = 0 , \quad (10)$$

$$\frac{\partial p(A, z)}{\partial z} + \rho g = 0 . \quad (11)$$

To finally specify the model, we need to describe the coronal pressure and density p and ρ. In a realistic model, p and ρ may be related to the temperature T by the ideal gas law,

$$p = R_0 \rho T , \quad (12)$$

where R_0 is the gas constant, and be subject to an equation of energy balance. To keep the model simple, we take a polytropic atmosphere where

$$p = \frac{P(A)}{z^n} , \quad (13)$$

$$\rho = \frac{n}{g}\frac{P(A)}{z^{n+1}} , \quad (14)$$

where P is a free function and n is a constant. Along each magnetic line of force, A is a constant and p is related to ρ by a polytropic power law. The ideal gas law gives a temperature

which increases linearly with height. This is not an unrealistic feature since one may expect an increase of the coronal temperature with height to some maximum beyond which the temperature decreases with heliocentric distance. In any case, our main interest lies not in the thermodynamics but in the magnetostatic structures of the model. The prescribed pressure and density automatically satisfy equation (11) describing the hydrostatic equilibrium along a line of force for any $P(A)$. What remains is then equation (10) for force balance across the magnetic field:

$$\nabla^2 A + Q\frac{dQ}{dA} + \frac{4\pi}{z^n}\frac{dP}{dA} + \frac{4\pi}{c} J_{\rm prom}(S)\delta(S) = 0 \qquad (15)$$

for prescribed forms of $Q(A)$, $P(A)$, and $J_{\rm prom}$, the last quantity being related by equation (7) to the prominence discrete mass m. In general, Q and P are nonlinear functions of A, and equation (15) is accordingly nonlinear. Moreover, one cannot simply prescribe a surface S and give $m(S)$. The source term $J_{\rm prom}$ given by equation (7) depends on the stream function A through the field component B_y on S, whereas A is the unknown of the problem. It is unclear whether solutions exist when the model is formulated in this manner. A logically consistent formulation of the problem is to leave S as an unknown and to prescribe m as a function of A, that is, in terms of the magnetic flux threading through the desired prominence sheet in the final solution, as discussed in Wu & Low (1987). This problem is not generally tractable. To avoid the above mathematical obstacles we examine the physical demands of the model and adopt a new approach.

2.2. *A Linear Model*

For the sake of rendering equation (15) linear, we set

$$Q = \lambda A^{1/2}\,, \qquad (16)$$

$$P = a_0 + a_1 A\,, \qquad (17)$$

where λ, a_0, and a_1 are constants. If the source term $J_{\rm prom}$ associated with the sheet located at $a < z < b$ on the z-axis is given (as a mathematical procedure), equation (15) becomes

$$\nabla^2 A = -\frac{1}{2}\lambda^2 - \frac{4\pi a_1}{z^n} - \frac{4\pi}{c} J_{\rm prom}(S)\delta(S)\,, \qquad (18)$$

a linear Poisson equation with a known source term. This equation can be solved for A subject to, say, a Dirichlet boundary condition as follows: For the domain $z > z_0$, the boundary value of A along $z = z_0$ gives the normal magnetic flux threading into the atmosphere from the solar surface. To complete the Dirichlet boundary condition, we demand that $|\nabla A|$ vanish at infinity in $z > z_0$. For consistency, the mass distribution $m(S)$ cannot be prescribed but is given *a posteriori* in terms of the prescribed $J_{\rm prom}$ and the field component B_y associated with the solution A. In this last step, it is not guaranteed that $m(S)$ so defined is positive definite, so that configurations with negative values of $m(S)$ must be rejected as unphysical. Despite this limitation, the model serves our physical purpose.

The general solution to equation (18) is a linear superposition of terms:

$$A = A_{\rm shear} + A_{\rm press} + A_{\rm prom} + A_{\rm pot}\,, \qquad (19)$$

where

$$\nabla^2 A_{\rm shear} = -\tfrac{1}{2}\lambda^2\,, \qquad (20)$$

$$\nabla^2 A_{\rm press} = -\frac{4\pi a_1}{z^n}\,, \qquad (21)$$

$$\nabla^2 A_{\rm prom} = -\frac{4\pi}{c} J_{\rm prom}(S)\delta(S)\,, \qquad (22)$$

$$\nabla^2 A_{\rm pot} = 0\,. \qquad (23)$$

The four terms on the right-hand side of equation (19) give the magnetic fields contributed by the field-aligned current, the pressure-induced cross-field current, the prominence current, and the currents external to the atmosphere, respectively. It is convenient to take $A_{\rm shear}$, $A_{\rm press}$, and $A_{\rm prom}$ to be fixed particular solutions to equations (20)–(22), leaving the potential stream function $A_{\rm pot}$ to be determined by the Dirichlet boundary condition on A. We set

$$A_{\rm shear} = \frac{\lambda^2}{8}\left[r_0^2 - y^2 - (z - r_0)^2\right]\,, \qquad (24)$$

$$A_{\rm press} = -\frac{4\pi a_1}{(n-2)(n-1)z^{n-2}}\,. \qquad (25)$$

The solution $A_{\rm shear}$ and the details of its derivation are given in Low (1993; hereafter Paper L). The solution $A_{\rm press}$ is an obvious particular solution to equation (21).

For a prescribed discrete current $J_{\rm prom}(S)$, a particular solution $A_{\rm prom}$ of equation (22) can be written down using the standard Green's function technique. In order to keep the mathematical development as simple as possible, we seek a candidate for which either $A_{\rm prom}$ or its magnetic field $\boldsymbol{B}_{\rm prom}$ is expressible in closed form. One possible candidate taken from Paper L is

$$B_{{\rm prom},y} - iB_{{\rm prom},z} = i\left[(\omega + ia')^{1/2} - (\omega + ib')^{1/2}\right]^2 + \frac{r_0^2}{\omega^3}\left[(a'\omega + ir_0^2)^{1/2} + (b'\omega + ir_0^2)^{1/2}\right]^2 + i\frac{(a'-b')^2}{4\omega}\,, \qquad (26)$$

in terms of positive constant parameters a' and b' and the complex variable $\omega = y + i(z - r_0)$. Note that the origin $\omega = 0$ corresponds to the point $y = 0$, $z = r_0$. The reason for introducing the constant displacement r_0 in the direction will become clear below. (In this and papers to follow, we will freely use the representation of potential fields by analytic functions of a complex variable, as described in the Appendix.) Equation (26) describes a magnetic field which is potential everywhere in $z > z_0 > 0$, except along the interval $z_0 < a < z < b$ on the z-axis with $a = r_0 - a'$ and $b = r_0 - b'$. Along this interval, the tangential component of the magnetic field reverses sign abruptly across the z-axis. This discontinuity in the magnetic field is associated with a discrete current flowing in the x-direction, given in terms of the magnetic field by Ampere's law:

$$J_{\rm prom}(S) = \frac{c}{4\pi}\left[B_{{\rm prom},z}(S)\right]_{y=0}\,, \qquad (27)$$

where the brackets indicate the discontinuous jump in the z-component of the magnetic field from $y < 0$ to $y > 0$. If this magnetic field were to be taken over the entire y-z plane, it is in fact the potential field due to the current sheet at $a < z < b$ and the image current sheet obtained by inversion about the circle $|\omega| = r_0$. Due to the image relationship between the two current sources, the circle $|\omega| = r_0$ is a line of force of the magnetic field, as previously noted in Paper L. This property

becomes important in § 2.3. For the present, the field given by equation (26) is just a candidate for a potential field contributed by the prominence sheet. Yet another candidate will be encountered in § 3.

Except for a final step, the construction of the model is basically complete since the only task remaining is to determine A_{pot} by using the Dirichlet boundary condition. Once the net stream function A is determined, equations (4) and (16) give $\boldsymbol{B}$, equations (13), (14), and (17) give the distribution of the coronal plasma, and equation (7) gives the self-consistent prominence mass distribution on the sheet S.

As noted in Paper L, the solution A_{shear} diverges to infinity for $(y^2 + z^2)^{1/2} \to \infty$ in $z > z_0$ and is thus unphysical if taken over the whole domain $z > z_0$. Another limitation comes from A_{press} which is associated with the presence of pressure gradients across the magnetic field. Equation (25) shows that the far regions $y \to \pm \infty$ at finite z are dominated by a horizontal magnetic field of finite strength, whereas we are interested in magnetic structures which are localized closed loops anchored to the photosphere $z = z_0$. These two undesirable features can be removed by limiting the presence of electric currents to a finite subdomain σ in $z > z_0$. This is accomplished by taking the functional forms Q and P given by equations (16) and (17) to apply only to a finite subdomain σ bounded by a magnetic line of force $A = A_0$, a constant. In the exterior, we take the atmosphere to be plane parallel with a potential magnetic field. While this removes unwanted physical features in the far region, the model is complicated by the need to solve for the shape of σ as a free boundary problem.

The complication arises from the inadequacy of the prescribed forms of Q and P in equations (16) and (17) to describe solutions taken over the infinite space. A more sophisticated prescription allowing for Q and P to take different forms in the near and far regions could avoid the free boundary problem, but the nonlinearity inherent in such an approach leads to generally intractable problems. The free boundary problem is actually a special case of this large class of nonlinear problems, namely, one in which the different forms of Q and P apply to regions separated by a sharp boundary.

Free boundary problems are nontrivial, and it is necessary to take an additional step in order to avoid having to solve this kind of problem in generality. We shall treat the region σ as given and seek particular solutions inside and outside of this region to be suitably matched at the boundary $A = A_0$. The boundary $A(y, z) = A_0$ is a free fluid boundary whose equilibrium requires the total pressure to be continuous across it (Spitzer 1967). The matching of the two solutions across this boundary leads naturally to a Cauchy boundary value problem for the Laplace equation, as we will see in § 2.3. Taking σ as given does not allow the arbitrary prescription of the Dirichlet boundary condition on $z = z_0$. For our purpose, there is no particular physical interest in the quantitative form of the normal magnetic flux at $z = z_0$, so this loss of freedom is not crucial.

2.3. *Atmosphere with Spatially Localized Volumetric Electric Currents*

Let us take the subdomain σ to be the region bounded by $z = z_0$ and a circular arc $\partial\sigma$ lying on the circle of radius r_0 centered at $y = 0$, $z = r_0$. The magnetic stream function has a free additive constant. With no loss of generality, set $A_0 = 0$ so that the line of force lying on $\partial\sigma$ is labeled $A = 0$. Exterior to σ, we have a potential field, with $Q = 0$, given by $A = A_{ext}$, where

$$\nabla^2 A_{ext} = 0 . \tag{28}$$

This potential field is embedded in a plane-parallel, hydrostatic atmosphere. To account for this exterior atmosphere, we replace equation (17)—originally defined for all space in $z > z_0$—with

$$\begin{aligned} P &= a_0 + a_1 A \quad \text{inside } \partial\sigma , \\ &= a_0 \quad\quad\quad \text{outside } \partial\sigma . \end{aligned} \tag{29}$$

The pressure and density in $z > z_0$ are then given by equations (13) and (14) with P defined by equation (29). With this choice of the constants a_0 and a_1 and the identification of $\partial\sigma$ with $A = 0$, the assumption is made that the plasma pressure is continuous across the magnetic surface $\partial\sigma$ where $A = 0$. The case of a discontinuous pressure across $\partial\sigma$ will be taken up in § 2.4. For the present case, the continuity of the total pressure implies that the magnetic field is continuous across $\partial\sigma$. Since $A = 0$ along $\partial\sigma$, this condition requires the normal derivative of A to be continuous across $\partial\sigma$.

We begin with the construction of a particular solution from which other solutions of the problem can be obtained by a procedure of linear superposition previously used in Paper L. This particular solution is constructed by continuing each of the terms in the linear superposition in equation (19) across $\partial\sigma$ to an exterior potential field in such a way that the net solution preserves $\partial\sigma$ as a line of force and has a continuous normal derivative across $\partial\sigma$. From Paper L, the nonpotential field A_{shear} obtaining in σ can be smoothly matched (with a continuous normal derivative) across the boundary $\partial\sigma$ to the exterior potential field

$$A_{shear,\,ext} = -\frac{\lambda^2}{8} r_0^2 \log\left[\frac{y^2 + (z - r_0)^2}{r_0^2}\right] . \tag{30}$$

Set

$$A_{ext} = A_{shear,\,ext} + A_{prom} , \tag{31}$$

fixing the potential field in the exterior of σ. The stream function A_{prom} is derived from the field given by equation (26). By virtue of its construction, this magnetic field has a line of force coinciding with $\partial\sigma$. Adjust the free constant of A_{prom} so that $A_{ext} = 0$ on $\partial\sigma$. The problem then reduces to determining the free potential field A_{pot} in equation (19) to ensure that the net field A matches the external potential field A_{ext}. Since the sum $A_{shear} + A_{prom}$ matches A_{ext} with continuous normal derivative at $\partial\sigma$, we arrive at the Cauchy-type boundary conditions on A_{pot} along $\partial\sigma$,

$$A_{pot} = -A_{press} , \tag{32}$$

$$\frac{\partial A_{pot}}{\partial r} = -\frac{\partial A_{press}}{\partial r} , \tag{33}$$

to determine A_{pot} in the domain σ governed by Laplace's equation (23). The normal derivatives are taken in the radial direction, denoted by r, from the center of the circle on which $\partial\sigma$ lies. Although this Cauchy problem is ill-posed, its solution exists (Courant & Hilbert 1963). The potential solution A_{pot} extrapolated from the Cauchy conditions is analytic except at certain points or regions of singularity intrinsic to the potential function itself. If these points or regions are located in $z < z_0$, outside of the domain of physical interest, A_{pot} is then analytic

in the physical domain, and the construction of the global magnetostatic solution is successful and complete. There are several subtle mathematical issues involved in this extrapolation whose pursuit we defer, to be taken up elsewhere. The point of physical relevance is that well-behaved solutions can be obtained in this manner; this will be shown by direct construction.

Once a particular global solution A has been constructed by the above method, new solutions can be obtained by its linear superposition with a potential field $A_{\rm image}$ taken over the entire domain $z > z_0$. This follows from the linearity of the equation governing A. To ensure that the boundary $\partial\sigma$ remains in equilibrium, the superposed potential field is required to have a line of force coinciding with this circular boundary. The requirement identifies the potential field $A_{\rm image}$ as generated by current singularities in the form of image pairs with respect to the circle of radius r_0 on which $\partial\sigma$ lies.

2.4. *The Cauchy Problem for the $n = 3$ Polytrope*

For illustration, we choose the $n = 3$ polytrope as a case soluble by analytic methods. We are interested in a potential function $A_{\rm pot}$ in σ satisfying the Cauchy conditions (32) and (33) on $\partial\sigma$. Change coordinates by the conformal (inversion) transformation $\xi + i\zeta = 1/(y + iz)$:

$$\xi = \frac{y}{y^2 + z^2}, \qquad \zeta = -\frac{z}{y^2 + z^2}. \tag{34}$$

The curves of constant ξ and ζ are two orthogonal families of circles tangent at the origin to the z- and y-axes, respectively. The circular boundary $\partial\sigma$ maps into the straight line $\zeta = -\zeta_0$ with $\zeta_0 = 1/2r_0$ in the ξ-ζ plane. The region σ is transformed into a region in the half-space $\zeta < -\zeta_0$. The Cauchy conditions (32) and (33) then transform into the conditions

$$A_{\rm pot} = \frac{2\pi a_1}{\zeta_0}(\zeta_0^2 + \xi^2), \tag{35}$$

$$\frac{\partial A_{\rm pot}}{\partial \zeta} = \frac{2\pi a_1}{\zeta_0^2}(\xi^2 - \zeta_0^2), \tag{36}$$

respectively, along the line $\zeta = -\zeta_0$, where we have set $n = 3$ and used equation (25).

Now $A_{\rm pot}$ is also potential in the ξ-ζ space, by the nature of conformal transformations. We therefore seek a potential function $A_{\rm pot}(\xi, \zeta)$ which satisfies equations (35) and (36). What makes this problem analytically soluble is that the expressions on the right-hand sides of these two equations are polynomials in ξ. Selecting from the set of potential functions which are polynomials in ξ and ζ, the desired solution is

$$A_{\rm pot} = \frac{2\pi a_1}{\zeta_0}(\xi^2 - \zeta^2 + 2\zeta_0^2) + \frac{2\pi a_1}{\zeta_0^2}\left\{\left[\xi^2(\zeta + \zeta_0) - \frac{1}{3}(\zeta + \zeta_0)^3\right] - 3\zeta_0^2(\zeta + \zeta_0)\right\}. \tag{37}$$

The two terms on the right-hand side enclosed by the braces are both potential functions. The first term takes care of boundary condition (35) since the second term vanishes at the same boundary; the second term ensures that boundary condition (36) is satisfied. Since the Cauchy initial values are polynomials in ξ, we are assured by the Cauchy-Kowalevsky Theorem (Courant & Hilbert 1963) that the extrapolation in the neighborhood of $\partial\sigma$ is unique. By the theory of analytic continuation, the extrapolation is also unique in the entire simply connected domain σ. It should be noted that the solution given by equation (37) is everywhere analytic except at $\xi = \infty, \zeta = \infty$, which corresponds to the origin $y = 0, z = 0$ in physical space. Hence, $A_{\rm pot}$ is well-behaved at all points in σ.

If we combine the terms $A_{\rm press}$ and $A_{\rm pot}$ in equation (19) into a single term, $A_{\rm corona} = A_{\rm press} + A_{\rm pot}$, then

$$A_{\rm corona} = \frac{2\pi a_1}{\zeta\zeta_0^2}(\zeta + \zeta_0)^2\left[\xi^2 - \frac{1}{3}\zeta(\zeta + 4\zeta_0)\right], \tag{38}$$

and the net stream function is given by

$$A = A_{\rm corona} + A_{\rm prom} + A_{\rm shear}, \tag{39}$$

in the current-flowing region σ; this solution matches smoothly with continuous first derivatives across the boundary $\partial\sigma$ to the exterior potential stream function $A_{\rm ext}$ defined by equation (31). Note that the function $A' = A - A_{\rm corona}$ in σ also matches smoothly with continuous first derivatives across $\partial\sigma$ to $A_{\rm ext}$. This implies that $A_{\rm corona}$ and its first derivatives vanish on $\partial\sigma$. This is obvious in equation (38), taking note that $\zeta = -\zeta_0$ on the circular boundary $\partial\sigma$. As pointed out above, we can linearly superpose a free potential function $A_{\rm image}$ globally to the above solution A, provided that $A_{\rm image}$ contains $\partial\sigma$ as a line of force so that boundary conditions (32) and (33) are unaffected. An infinite family of magnetostatic solutions can thus be generated.

2.5. *Pressure Discontinuity at $\partial\sigma$*

If the pressure is not continuous at $\partial\sigma$, replace equation (29) with

$$\begin{aligned} P &= a_0 + a_1 A \quad \text{inside } \partial\sigma, \\ &= b_0 \quad\quad\;\; \text{outside } \partial\sigma, \end{aligned} \tag{40}$$

where $b_0 \neq a_0$ is a constant. To ensure the continuity of the total pressure across $\partial\sigma$, the magnetic field must be discontinuous at this surface so that the jump in magnetic pressure compensates for the jump in plasma pressure, giving

$$\left[\frac{B^2}{8\pi}\right]_{\partial\sigma} = \frac{a_0 - b_0}{z^3}, \tag{41}$$

where the brackets indicate a jump in value across $\partial\sigma$ from the inside. When $b_0 = a_0$, this condition reduces to requiring $\boldsymbol{B}$ to be continuous, or the derivatives of A to be continuous, across $\partial\sigma$. For this special case, boundary condition (41) is linear in A. When $b_0 \neq a_0$, boundary condition (41) is nonlinear in A and it puts a restriction on the use of linear superposition of solutions to generate new ones, as we shall see.

For the purpose of illustration, let us take $A_{\rm corona}$ alone, given by equation (38), to be the stream function for a magnetic field confined in σ and seek a potential field $\boldsymbol{B}_{\rm jump}$ with stream function $A_{\rm jump}$ outside of σ which satisfies boundary condition (41). Since the derivatives of $A_{\rm corona}$ vanish at $\partial\sigma$, where $A_{\rm corona} = 0$, it follows that $A_{\rm jump} = 0$ and

$$\left(\frac{\partial A_{\rm jump}}{\partial r}\right)^2 = \frac{8\pi(a_0 - b_0)}{z^3} \tag{42}$$

along $\partial\sigma$, posing a Cauchy boundary value problem for $A_{\rm jump}$ in the region outside of σ in $z > z_0$.

Transform the Cauchy boundary value problem from physical space into the ξ-ζ plane. The circle coincident with $\partial\sigma$ has the image $\zeta = -\zeta_0$. The region outside of σ lies in $\zeta > -\zeta_0$ in the image space. Writing $A_{\rm jump}$ as a function of ξ and ζ, the transformed boundary conditions are $A_{\rm jump} = 0$ and

$$\frac{\partial A_{\rm jump}}{\partial \zeta} = \left[\frac{8\pi(a_0 - b_0)}{\zeta_0^2}\right]^{1/2} (\zeta_0^2 + \xi^2)^{1/2} \tag{43}$$

along $\zeta = -\zeta_0$. The Cauchy boundary value problem cannot be solved by the simple method of § 2.4. We employ a different method based on the technique of analytic continuation, which deals with the magnetic field instead of the stream function. Once the magnetic field is known, the stream function if needed can be obtained by a simple integration. Although the method in § 2.4 is intuitively transparent, the method based on analytic continuation has quite general application as will be obvious from its use below.

It is convenient for later discussion to suppress the dependence of the amplitude of $A_{\rm jump}$ on a_0 and b_0 by writing

$$A_{\rm jump} = B_0 \Psi , \tag{44}$$

where B_0 is a constant which in the present problem is given by

$$B_0^2 = 8\pi(a_0 - b_0) . \tag{45}$$

We therefore have the potential field

$$\boldsymbol{B}_{\rm jump} = B_0\left(\frac{\partial \Psi}{\partial z}\,\hat{y} - \frac{\partial \Psi}{\partial y}\,\hat{z}\right). \tag{46}$$

In the ξ-ζ plane, Ψ defines a potential vector field

$$\boldsymbol{H}(\xi, \zeta) = H_\xi \hat{\boldsymbol{\xi}} + H_\zeta \hat{\boldsymbol{\zeta}} , \tag{47}$$

where

$$H_\xi = \frac{\partial \Psi}{\partial \zeta} , \quad H_\zeta = -\frac{\partial \Psi}{\partial \xi} . \tag{48}$$

The chain rule of differentiation and the Cauchy-Riemann relations (see the Appendix) can be used to show that

$$B_{{\rm jump},y} - iB_{{\rm jump},z} = B_0(H_\xi - iH_\zeta)\left(\frac{\partial \zeta}{\partial z} + i\,\frac{\partial \zeta}{\partial y}\right), \tag{49}$$

giving the magnetic field generated by $A_{\rm jump}$ in physical space. The boundary condition $A_{\rm jump} = 0$ and equation (43) taken at $\zeta = -\zeta_0$ translate into

$$H_\xi = \frac{1}{\zeta_0^{3/2}} (\zeta_0^2 + \xi^2)^{1/2} , \quad H_\zeta = 0 , \tag{50}$$

along $\zeta = -\zeta_0$. The potential field $\boldsymbol{H}$ has the representation

$$H_\zeta - iH_\xi = W(w) , \tag{51}$$

where W is an analytic function of the complex variable $w = \xi + i\zeta$. The problem thus becomes one of looking for an analytic function in the complex plane w such that its value on the line $\zeta = -\zeta_0$ is given by equation (50), a classical problem of analytic continuation which has a unique solution. By inspection of equations (50) and (51), it is obvious that the solution to the problem is

$$H_\xi - iH_\zeta = \frac{1}{\zeta_0^{3/2}} \{\zeta_0^2 + [\xi + i(\zeta + \zeta_0)]^2\}^{1/2} . \tag{52}$$

Using equation (49), the potential field $\boldsymbol{B}_{\rm jump}$ in physical space can be constructed in the final step.

As shown in the Appendix, the stream function $A_{\rm jump} = B_0 \Psi$ can be integrated from the vector field $\boldsymbol{H}$ in the complex plane of w, giving

$$A_{\rm jump} = B_0 \frac{1}{2\zeta_0^{3/2}} \,{\rm Im}\left\{[w(\zeta_0^2 + w^2)]^{1/2} + \zeta_0^2 \sinh^{-1}\left(\frac{w}{\zeta_0}\right)\right\}, \tag{53}$$

where Im denotes the imaginary part of a complex quantity. In the construction of explicit solutions in the next section, we shall use equations (49) and (52) to define the magnetic field and numerically integrate for $A_{\rm jump}$ in the y-z plane. This approach is preferred over the analytical form for $A_{\rm jump}$ given by equation (53) because it involves simpler rules to define the branch cuts associated with complex functions in order to obtain the correct magnetic topology.

For a given pressure discontinuity on $\partial\sigma$ fixed by the constants a_0 and b_0 in equation (41), the potential field $\boldsymbol{B}_{\rm jump}$ obtaining in the exterior of σ matches the interior solution $A_{\rm corona}$ at $\partial\sigma$ with a jump in magnetic pressure, while preserving the continuity of the total pressure. By definition, $a_0 > b_0$, as is evident from equation (45) defining the amplitude B_0 of $\boldsymbol{B}_{\rm jump}$. This also follows from the fact that $\boldsymbol{B}_{\rm jump}$ is zero in σ and increases discontinuously across $\partial\sigma$ to nonzero values outside, whereas the nonpotential field $\boldsymbol{B}_{\rm corona}$ introduces no discontinuity across $\partial\sigma$. It is the excess magnetic pressure in the exterior which requires an enhanced pressure in σ, i.e., $a_0 > b_0$, to balance it.

3. EXPLICIT SOLUTIONS

To survey the rich variety of solutions this model provides, we present a series of illustrative examples in order of increasing complexity.

3.1. *The $A_{\rm corona}$ Solution*

The magnetic field generated by $A = A_{\rm corona}$ shown in Figure 1 is composed of three bipolar fields with an X-type magnetic neutral point on the z-axis. The solid and dashed curves of constant A correspond to positive and negative values of A, respectively. This magnetic field is symmetric about the z-axis and is entirely confined (by the pressure and weight of the $n = 3$ polytropic atmosphere) within the circularly shaped region σ marked by the line of force $A = 0$. The line $A = 0$ lies on the circle $\zeta(y, z) = -\zeta_0$ of radius r_0 centered at $y = 0$, $z = r_0$. The X-type neutral point is located at $y = 0$, $z = (2/3)r_0$, below the center of this circle, as can be verified by direct calculation using the formula for $A_{\rm corona}$. Outside of σ, the atmosphere is unmagnetized and in plane-parallel hydrostatic equilibrium. In the magnetic region, density is depleted relative to that hydrostatic atmosphere at the same height everywhere, except over the central bipolar field (below the X-type neutral point where density is enhanced. Figure 2 shows the density departure from the plane-parallel values at the same height. Direct calculation shows that the line of force of the central bipolar field, forming a boundary between density depletion and enhancement, intersects the z-axis at $z = (1/2)r_0$, a point halfway between the origin and the center of the circle $\zeta(y, z) = -\zeta_0$. Because the magnetic field goes zero smoothly across $A = 0$, no sharp density boundary is visible.

It is instructive to compare this magnetic field with the potential field having the same boundary flux distribution at

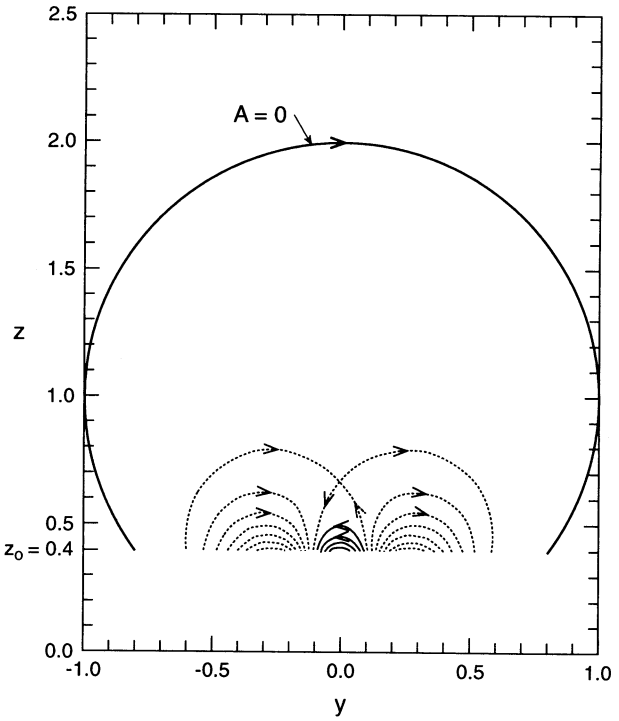

FIG. 1.—Magnetic field generated by $A = A_{corona}$ in the domain $z \geq z_0 = 0.4$. Contours with positive and negative values of A are drawn with solid and dashed lines, respectively, with arrows marking the direction of the field. The field is confined in the circle $\zeta = -1/2r_0$ with $r_0 = 1$ marked by $A = 0$. Exterior to this circle, the field is everywhere zero.

the base $z = z_0$, shown in Figure 3. This field is generated by the stream function

$$A_{corona,pot}(y, z) = -\frac{1}{\pi}\int_{-\infty}^{\infty} \frac{(z - z_0)A_{corona}(y', z_0)}{(y - y')^2 + (z - z_0)^2}\, dy' \qquad (54)$$

and has a different field line connectivity as evidenced by the location of the X-type neutral point on a different line of force. The lines of force in Figures 1 and 3 are plotted for the same set of values of the stream functions. The difference in magnetic topology is readily seen by laying a transparent copy of one over the other. The potential field in Figure 3 permeates all parts of the atmosphere which is everywhere in plane-parallel hydrostatic equilibrium. The magnetic field in Figure 1 is clearly in a state of much higher energy since the magnetic field is spatially confined. This kind of magnetostatic structure arises in the course of solar activity because the magnetic field emerges initially from below the corona.

The complete absence of magnetic field outside the region σ is artificial. We can superpose A_{corona} with a potential field, provided the latter preserves $A = 0$ as the same circular line of force. One such potential field is the dipole potential field

$$A_{dipole} = \zeta + \zeta_0 \,. \qquad (55)$$

Figures 4–6 show the magnetic field obtained by the linear superposition: $A = A_{corona} + a_{dipole} A_{dipole}$, for three increasing positive values of the amplitude a_{dipole}. The dipole potential field extends beyond the boundary $A = 0$ so that the magnetic field is no longer zero outside $A = 0$. If $a_{dipole} > 0$, the linear superposition enhances the central bipolar field in Figure 1. For a moderate value of $a_{dipole} > 0$, such as the case shown in Figure 4, a shell-like region where $A > 0$ forms just inside of $A = 0$. Since the density differential $\Delta\rho \propto A/z^4$, this shell-like

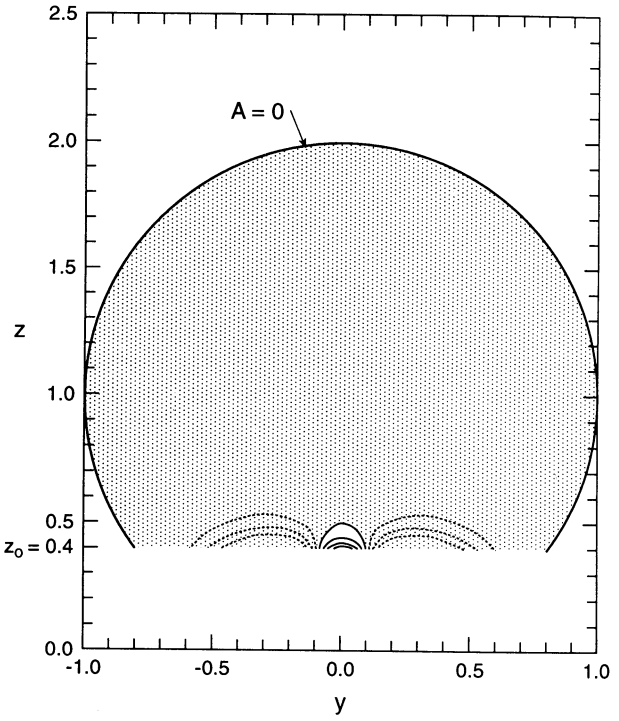

FIG. 2.—Contours of constant density departure from a reference plane-parallel hydrostatic density at the same height: $\Delta\rho \propto A_{corona}/z^4$. Contours of positive and negative values of $\Delta\rho$ are drawn with solid and dashed lines, respectively. Outside of the circle $A = 0$, $\Delta\rho$ is zero everywhere.

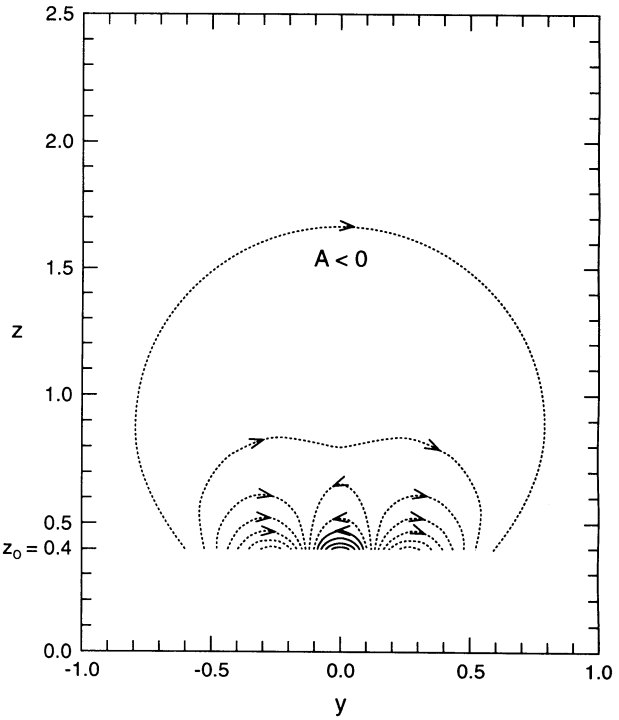

FIG. 3.—Potential magnetic field in $z \geq z_0 = 0.4$ with the same boundary values of A on $z = z_0$ as the nonpotential field shown in Fig. 1. Contours are drawn for those same A-values found in Fig. 1. Note that the contour $A = 0$ runs along $z = z_0$ because this potential field fills all space in $z > z_0$.

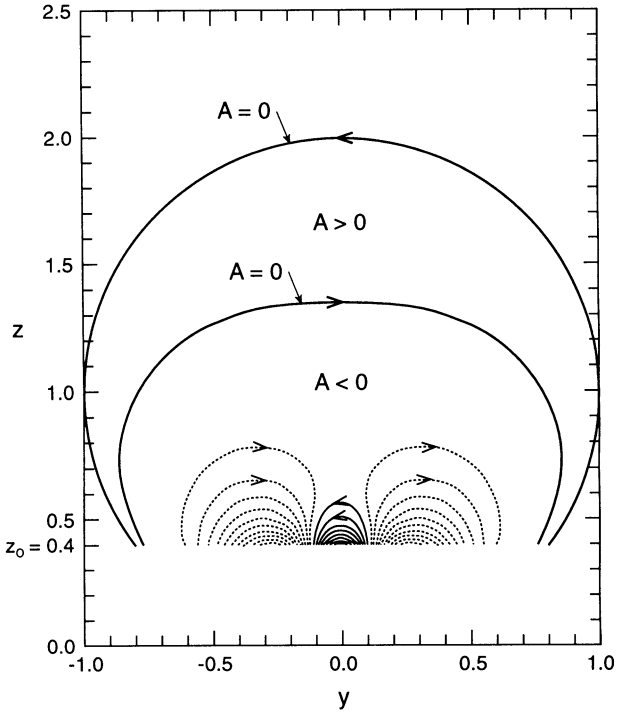

FIG. 4.—Magnetic field $A = A_{\text{corona}} + 0.4\zeta$

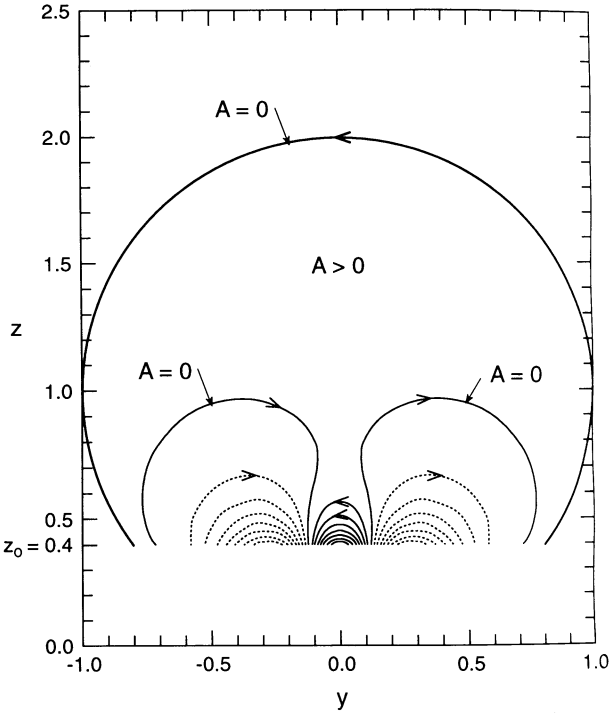

FIG. 5.—Magnetic field $A = A_{\text{corona}} + 0.8\zeta$

region shows a density enhancement above a reference background hydrostatic atmosphere. Enclosed by this shell is the cavity of density depletion seen previously in Figure 1 but now reduced in size. The original density enhancement associated with the central bipolar field seen in Figure 1 has at the same time grown in geometric size in Figure 4. Here and for other examples to follow, we omit separate displays of the contours of $\Delta\rho$ since these can be inferred readily from the contours of A, given the linear relationship between these two quantities.

As the amplitude a_{dipole} increases, the above two regions of positive A increase their geometric sizes parametrically, to eventually merge, as shown in Figure 5, splitting the density depletion ($A < 0$) region into two. For a sufficiently large a_{dipole}, such as the case in Figure 6, the central bipolar field dominates completely and density is enhanced everywhere in σ.

If $a_{\text{dipole}} < 0$, the added dipole potential field reduces the central bipolar field in Figure 1. This has the effect of reducing the central density enhancement associated with this bipolar field and enlarging the density depletion region. We omit presenting an explicit example of this less interesting case.

To understand the above density distributions, note from equations (4) and (21) that the current density in the atmosphere is given by

$$\nabla \times \boldsymbol{B} = \frac{4\pi a_1}{z^3}\,\hat{\boldsymbol{x}}\,, \tag{56}$$

where we have set $n = 3$ and set all stream functions on the right-hand side in equation (19) to zero except for the contribution A_{corona}. The current density is everywhere positive and in the x-direction. Consider force balance in terms of a hydrostatic relation between pressure and density *along*, and the Lorentz force everywhere directed *perpendicular to*, the lines of force; see equation (9). Given the sign of the magnetic field contributed by $A = A_{\text{corona}}$ shown in Figure 1, the Lorentz force is directed out of the region σ except in the central bipolar field. The outward Lorentz force is balanced principally by an inwardly directed pressure gradient in the density depletion region. In the density enhancement region of the central bipolar field, the pressure gradient is directed outward to

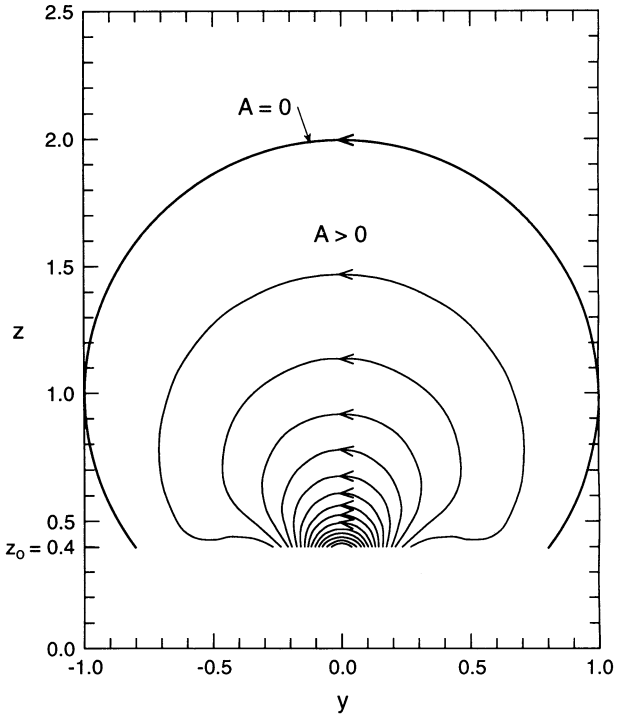

FIG. 6.—Magnetic field $A = A_{\text{corona}} + 5\zeta$

balance the inward, confining Lorentz force. The superposition with the potential dipole field does not change the current density. On the other hand, the Lorentz force is modified because of the addition of a potential field. Depending on whether the regions of outward and inward Lorentz forces are enlarged or contracted, the respective regions of density enhancement and depletion are similarly changed, as shown in Figures 4, 5, and 6.

3.2. *Sheared Magnetic Fields*

Consider now the superposition: $A = A_{\rm corona} + a_{\rm shear} A_{\rm shear}$, $a_{\rm shear}$ being a constant amplitude, which introduces currents aligned with the magnetic field. This superposition produces a component of current density in the x-direction, uniformly distributed over σ, in addition to that given by equation (56):

$$(\nabla \times \boldsymbol{B})_x = \frac{4\pi a_1}{z^3} + \frac{1}{2}\lambda^2 ; \qquad (57)$$

see equations (4), (20), and (21). The net field is sheared with a nonvanishing component in the x-direction in the region σ, a point to be borne in mind when viewing lines of force projected on the y-z plane. This component of the field has the effect of an isotropic magnetic pressure; see Paper L. This pressure force provides a means, in addition to that derived from the plasma pressure, to balance the Lorents force in the y-z plane. The relationship between the Lorentz force and the distribution of the plasma density becomes more complicated than that found in the unsheared magnetic fields of § 3.1.

Before we proceed, a warning is needed. The stream function A can take on negative values in σ rendering the x-component of the field defined by equation (16) imaginary. This can be remedied by replacing equation (16) by

$$Q = \lambda(A_0 + A)^{1/2} , \qquad (58)$$

where the constant A_0 is chosen such that the square root is real in σ. The solution $A_{\rm shear}$ continues to satisfy the governing equation (Paper L). However, this would present the complication that Q jumps discontinuously from a finite value to zero upon crossing the boundary $A = 0$. Force balance at this boundary requires the continuity of the magnetic pressure across it. Since $Q = \lambda A_0^{1/2}$, a constant on the boundary, and both $A_{\rm shear,ext}$ and $A_{\rm shear}$ give uniform tangential fields along $A = 0$, a suitable choice of the amplitude of $A_{\rm shear,ext}$ ensures continuity of magnetic pressure across $A = 0$. In the following, we bear in mind that this extension of the model has been made wherever A takes on negative values in σ.

The magnetic field generated by $A_{\rm shear}$ alone is a twisted rope of magnetic flux running parallel to the x-axis. Where it dominates, it produces closed, projected magnetic loops in the y-z plane. Figure 7 shows an example of the superposition of $A_{\rm corona}$ and $A_{\rm shear}$ with the circulation of the magnetic flux rope in the same sense as the central bipolar field in Figure 1. A detached set of magnetic loops forms in the upper region of σ, indicating the presence of a magnetic flux rope. This flux rope is a region of density enhancement ($A > 0$). The pressure of the enhanced plasma and the isotropic pressure of the x-component of $\boldsymbol{B}$ are both confined by the closed magnetic loops (in the y-z plane) of the rope. On the other hand, the weight of the enhanced plasma is supported partially by the Lorentz force associated with the compression on the magnetic field below. The magnetic field extends outside the region σ, contributed in that part of the domain by $A_{\rm shear,pot}$.

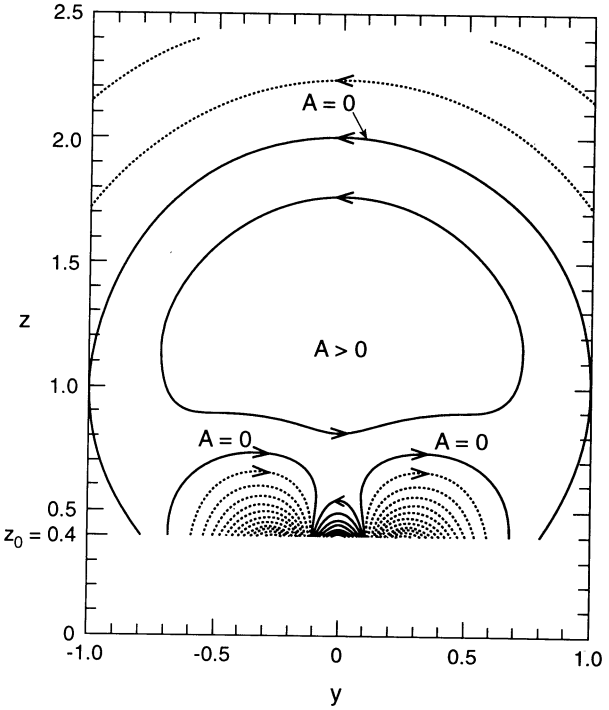

FIG. 7.—Magnetic field $A = A_{\rm corona} + A_{\rm shear}$. The field in the current-flowing region bounded by $A = 0$ is sheared with $B_x \neq 0$.

Figure 8 shows the configuration for the case where the same $A_{\rm corona}$ is superposed with $A_{\rm shear}$ of the opposite sign. For an amplitude such that the latter dominates in the upper region of σ, the flux rope of the opposite twist forms a region of density depletion. The inward plasma pressure force together with the

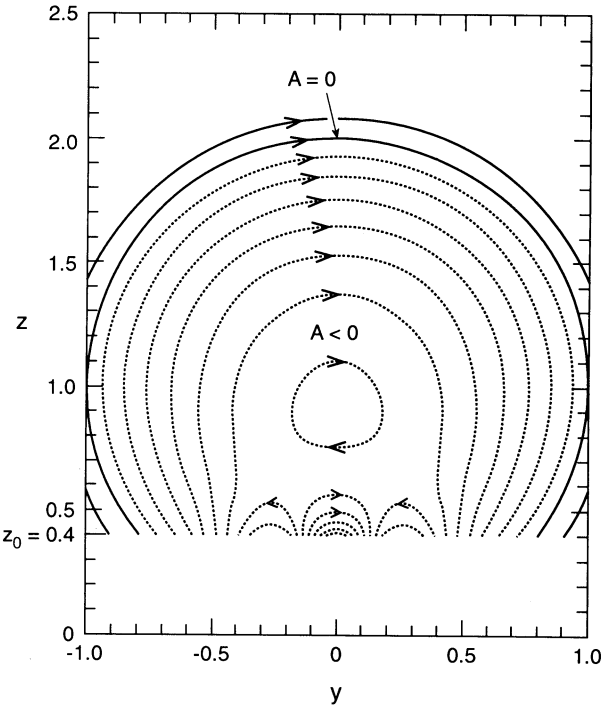

FIG. 8.—Magnetic field $A = A_{\rm corona} - 7A_{\rm shear}$. The field in the current-flowing region bounded by $A = 0$ is sheared with $B_x \neq 0$.

Lorentz force associated with the closed magnetic loops confine the isotropic pressure of the x-component of $\boldsymbol{B}$. This depleted region is buoyant in the stratified atmosphere and is seen in the equilibrium state to be straining upward against the confining magnetic lines of force anchored to the base $z = z_0$.

These two basic types of magnetostatic configurations can be further modified by superposing them with the dipole potential field $A_{\rm dipole}$ which preserves the special line of force $A = 0$. We leave the reader to explore these possibilities. The addition of $A_{\rm dipole}$ changes the distribution of the Lorentz force in the y-z plane by changing the magnetic field distribution without changing the current density in the x-direction.

3.3. *Pressure Discontinuity at $\partial\sigma$*

It is instructive to first visualize the vector field $\boldsymbol{H}$ in the ξ-ζ plane given by equation (52) and shown in Figure 9. This field is obtained by writing equation (52) in the form

$$H_\xi - iH_\zeta = \frac{1}{\zeta_0^{3/2}} (\xi + i\zeta)^{1/2}[\xi + i(\zeta + 2\zeta_0)]^{1/2} , \qquad (59)$$

taking the respective branch cuts of the two square roots from $\zeta = 0$ to ∞ and from $\zeta = -2\zeta_0$ to $-\infty$, along the ζ-axis, as indicated in Figure 9. The field $\boldsymbol{H}$ is tangential along the cuts and changes sign abruptly across it. These cuts may be interpreted to be electric current sheets in the ξ-ζ plane. These currents sheets as sources of the field $\boldsymbol{H}$ are images relative to the line $\zeta = -\zeta_0$. Hence, $\boldsymbol{H}$ is symmetric about $\zeta = -\zeta_0$ and is tangential along this line. It is this property which is preserved by the conformal transformation (34) of $\boldsymbol{H}$ into $\boldsymbol{B}_{\rm jump}$ in physical space. In the transformation, the line $\zeta = -\zeta_0$ becomes the circular boundary $\partial\sigma$ coinciding with the line of force $A = 0$ of the physical magnetic field. The cuts $0 < \zeta < \infty$ and $-2\zeta_0 > \zeta > -\infty$ in the ξ-ζ plane map into two current sheets on the z-axis, respectively running from $z = 0$ to $-\infty$ and $z = 0$ to r_0, where $\zeta_0 = 1/2r_0$ and r_0 is the radius of the circle on which $\partial\sigma$ lies. The latter two current sheets form an image pair with respect to the circle $\zeta(y, z) = -\zeta_0$. It is this geometry of the current distribution which produces a line of force coinciding with $\zeta(y, z) = -\zeta_0$. For the same reason, the field $\boldsymbol{B}_{\rm prom}$ given by equation (26) has a circular line of force $A_{\rm prom} = 0$.

Figure 10 shows the lines of force of $\boldsymbol{B}_{\rm jump}$ taken over all space in $z > z_0$. Only the part of the second current sheet, extending from $z = 0$ to $z = r_0$, located in $z > z_0$ is shown. It is interesting to note that this current sheet is not threaded by the magnetic field, so that if it is admitted in the model, it is force-free.

The essence of the construction in § 2.5 is that the magnetostatic solution described in Figures 1 and 2 can be combined with $\boldsymbol{B}_{\rm jump}$ to describe a global atmosphere. Inside $\partial\sigma$, the magnetic field and density are as given in Figures 1 and 2. Outside $\partial\sigma$, the atmosphere is permeated by the magnetic field $\boldsymbol{B}_{\rm jump}$ and is in hydrostatic equilibrium with a plane-parallel pressure

$$p = \frac{b_0}{z^3} . \qquad (60)$$

The part of the magnetic field $\boldsymbol{B}_{\rm jump}$ inside $\partial\sigma$ is irrelevant in this construction. In this global solution, $\partial\sigma$ is in force equilibrium with a continuity of total pressure across it as described by equation (41), with $a_0 > b_0$. Hence, there is a discontinuous increase in the pressure and density upon crossing $\partial\sigma$ from the exterior. Inside $\partial\sigma$, the density shows both enhancement and depletion as the result of the electric currents associated with $A_{\rm corona}$, as displayed in Figure 2.

This particular solution can be generalized. Redefine the potential field $\boldsymbol{B}_{\rm jump}$ to be nonzero everywhere in $z > z_0$, setting

$$\begin{aligned} A_{\rm jump} &= B_{\rm in}\Psi \quad \text{inside } \partial\sigma , \\ &= B_{\rm out}\Psi \quad \text{outside } \partial\sigma , \end{aligned} \qquad (61)$$

where $B_{\rm in}$ and $B_{\rm out}$ are constant amplitudes. The magnetic field $\boldsymbol{B}_{\rm jump}$ alone describes a simple atmosphere. Since $\boldsymbol{B}_{\rm jump}$ is potential everywhere except at $\partial\sigma$, take the atmosphere to have

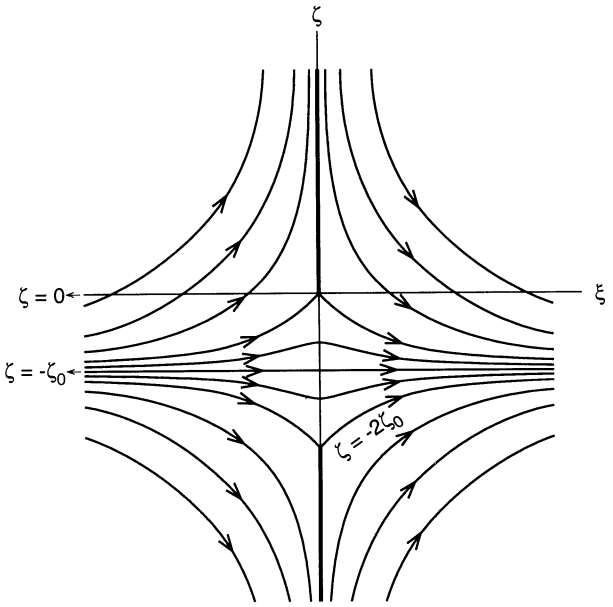

FIG. 9.—Flow lines of the vector field $H_\xi - iH_\zeta$ in the ξ-ζ plane given by equation (59). The thick lines on the ζ-axis, extending from $\zeta = 0$ to ∞, and from $\zeta = -2\zeta_0$ to $-\infty$, are the branch cuts described in the text, across which a tangential $\boldsymbol{H}$ reverses sign abruptly.

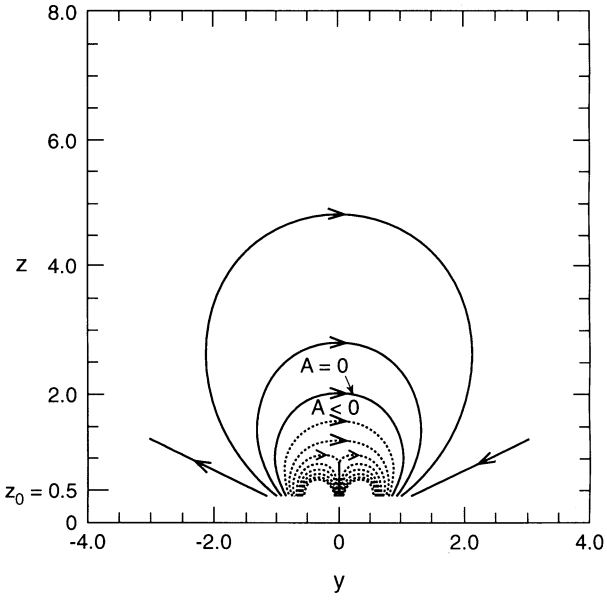

FIG. 10.—Lines of force of $\boldsymbol{B}_{\rm jump}$ taken over the y-z plane in $z > z_0$. The line of force $A = 0$ corresponds to the circle $\zeta = -1/2r_0$ of radius r_0 centered at $y = 0$, $z = r_0$; here $r_0 = 1$. This magnetic field is potential everywhere except on the z-axis in the interval $r_0 > z > z_0$ where $\boldsymbol{B}_{\rm jump}$ is tangential and has opposite signs on the opposite sides of this line segment.

the plane-parallel pressures

$$p = \frac{a_0}{z^3} \quad \text{inside } \partial\sigma\,, \qquad = \frac{b_0}{z^3} \quad \text{outside } \partial\sigma\,. \tag{62}$$

The only currents in the atmosphere are in the vertical current sheet extending from the base $z = z_0$ to $z = r_0$ on the z-axis, and in the boundary $\partial\sigma$. As we have pointed out, the former is force-free. Along $\partial\sigma$, the pressure jump across it arising from $a_0 \neq b_0$ in equation (62) can be balanced by the jump in the magnetic pressure. Using equation (41), we obtain

$$\frac{1}{8\pi}(B_{\text{out}}^2 - B_{\text{in}}^2) = a_0 - b_0\,, \tag{63}$$

relating the two amplitudes B_{in} and B_{out} to the pressure discontinuity. Now the region σ can have high ($a_0 > b_0$) or low ($a_0 < b_0$) density relative to the exterior, depending on whether it contains an enhanced or reduced magnetic field relative to the exterior.

The nonlinearity of the jump condition (41) restricts severely the linear superposition of solutions to generate new ones. For example, the superposition of A_{jump} with a global potential stream function A_{image} to preserve $\partial\sigma$ as a line of force does not satisfy the jump condition (41), a situation quite in contrast to the case where pressure is continuous across $\partial\sigma$. Linear superposition with A_{jump} is possible only with a stream function whose magnetic field vanishes on $\partial\sigma$ and thus does not contribute to equation (41). The nonpotential field A_{corona} satisfies this requirement. Figure 11 shows a superposition of A_{jump} given by equation (61) and A_{corona}. The presence of the field due to A_{corona} in σ gives rise to two features: First, the plasma pressure in σ is described by equation (41) with $a_1 \neq 0$ instead of equation (62); the electric currents contributed by A_{corona} gives rise to departure from plane-parallel distribution. Second, the vertical current sheet of $\boldsymbol{B}_{\text{jump}}$ is now threaded by the magnetic field contributed by A_{corona}.

In Figure 11, we have a superposition in which the Lorentz force on the current sheet is directed upward in the upper part of it. This force can be balanced by the gravitational force according to equation (7) for a suitable mass distribution. Figure 11 as a crude model has several qualitative features resembling the three-part structure of the coronal helmet. Setting $B_{\text{out}} > B_{\text{in}}$, and by equation (63), $a_0 > b_0$, we find a discontinuous increase in density across $\partial\sigma$ from the outside, which can be identified with the high-density helmet. The density shows depletion inside $\partial\sigma$ ($A < 0$ within σ in Fig. 11); this may be identified with the prominence cavity. Finally, the current sheet suspended by a discrete Lorentz force may be identified with the prominence. There are limitations, of course. Most serious is that the boundary $\partial\sigma$ is unstable for $a_0 > b_0$, a point we will address in § 3.4. In addition, the density depletion region in σ is not, contrary to observation, separated from the high-density region by a sharp boundary, and the prominence extends to the lower boundary $z = z_0$ rather than being wholly suspended in the atmosphere. In fact, as shown in Figure 11, in the lower part of the whole current sheet extending from $z = 0$ to $z = (2/3)r_0$, the Lorentz force is acting downward. This part of the current sheet is not physically admissible since gravity is the only means of balancing the Lorentz force on the sheet. For this reason, we set the boundary $z = z_0 = (2/3)r_0$ at a level which excludes the unphysical lower portion of the current sheet. In the next paper of the series dealing with prominences, models will be presented with physically more reasonable prominence sheets, namely, those wholly suspended in the atmosphere.

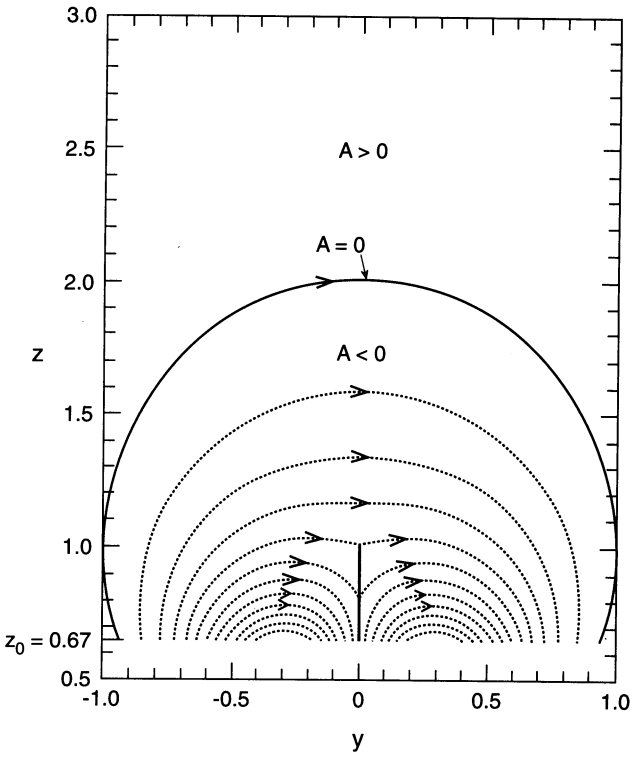

FIG. 11.—Magnetic field generated by a linear superposition of A_{corona} with A_{jump}, the latter given by equation (61). Exterior to the circular line of force $A = 0$, the magnetic field is potential. Across $A = 0$ from the exterior, the magnetic intensity is reduced discontinuous with a corresponding increase of pressure to maintain continuity of the total pressure. The negative values of A indicated by dashed contours inside $A = 0$ implies a density reduction $\Delta\rho \propto A/z^4$ relative to a plane-parallel atmosphere compatible with the pressure jump along $A = 0$. The thick vertical line along the z-axis extending from the base of the atmosphere represents a prominence sheet suspended by the magnetic field threading through the sheet. The base $z = z_0$ has been set at $z_0 = (2/3)r_0$ with $r_0 = 1$.

3.4. *Stability of the Discontinuity at $\partial\sigma$*

The availability of explicit, equilibrium solutions presents an opportunity to study their mechanical stability to small amplitude perturbations. Although stability analysis lies outside the scope of our paper, one aspect of it is interesting and relatively simple to demonstrate, namely, the stability or instability of the discontinuity at $\partial\sigma$.

Consider the magnetostatic atmosphere with the magnetic field $\boldsymbol{B}_{\text{jump}}$ generated by the stream function given by equation (61). Although the total pressure is continuous across $\partial\sigma$, its derivative is not. The jump of the total pressure force determines the stability of $\partial\sigma$. The energy principle states that this boundary is stable if and only if the change in the potential energy of the system

$$\delta E = \int_{\partial\sigma} \left[\nabla\left(p + \frac{B^2}{8\pi}\right)\cdot\hat{\boldsymbol{r}}\right]_{\partial\sigma} \eta^2\, ds \tag{64}$$

is positive definite for all infinitesimal displacement η in the direction $\hat{\boldsymbol{r}}$ normal to the boundary (Bernstein et al. 1958;

Spitzer 1967). In equation (64), ds is the line element on $\partial\sigma$ and the square brackets indicate the jump of the gradient upon crossing $\partial\sigma$ in the positive direction of $\hat{r}$. Direct evaluation gives

$$\delta E = \frac{(b_0 - a_0)}{\zeta_0^4} \int_{\partial\sigma} (\xi^2 + \zeta_0^2)^3 (3\xi^2 + \zeta_0^2)\eta^2 \, ds \, . \qquad (65)$$

This shows that the boundary $\partial\sigma$ is stable if and only if the region σ is depleted of density relative to the exterior with $b_0 > a_0$. Hence, as a model of the helmet which has a high density relative to its exterior, the magnetostatic state given by equation (61) is physically not admissible because the boundary $\partial\sigma$ is unstable. Conversely, as a model of the prominence cavity embedded in the high density of the helmet, this state is admissible by reason of stability.

This stability result is a particular example of a general result due to Hu (1988). In that work, a general class of magnetostatic equilibrium was considered, obtained by modifying the magnetic field intensity of a given potential field $\boldsymbol{B}_p$ without changing the field geometry, and introducing pressure gradients and a density distribution to ensure a balance among the Lorentz, pressure, and gravitational forces. The equilibrium atmosphere associated with the magnetic field given by equation (61) is, in fact, a member of this class of equilibria. Hu showed in generality that the stability of each of these equilibria depends crucially on the gradients $\nabla_\perp(|\boldsymbol{B}|)$ and $\nabla_\perp(|\boldsymbol{B}_p|)$ perpendicular to gravity: stability obtains if and only if the specific gradient of the modified field intensity $\nabla_\perp(|\boldsymbol{B}|)/|\boldsymbol{B}|$ is of the same sign and steeper than the corresponding gradient for the unmodified potential field. In our particular example, this specific gradient is made more steep at $\partial\sigma$ than in the potential field (obtaining from equation (61) with $B_{\rm in} = B_{\rm out}$, i.e., with no discontinuity at $\partial\sigma$) when $b_0 > a_0$.

The principal stabilizing influence of coronal structures is the anchoring of the magnetic field in the dense photosphere; rigid anchoring is assumed in the criterion involving δE given by equation (64) (Low 1990). Under this influence, the stability of the surface $\partial\sigma$ is determined by a competition between the forces arising from magnetic curvature and density stratification (Low 1985; Hu 1988). If $b_0 > a_0$, the case of σ being a density cavity, the relatively high magnetic field in σ is convex to the high-density exterior. The magnetic curvature force associated with $\partial\sigma$ is stabilizing everywhere on $\partial\sigma$. Along the upper half of the circular boundary $\partial\sigma$, dense plasma sits above the less dense plasma inside σ. This part of the boundary is Rayleigh-Taylor unstable but is dominated by the stabilizing effect of the magnetic curvature force. Along the lower half of $\partial\sigma$, the density stratification is stable, and it enhances the stability of this part of the boundary. Hence the entire boundary $\partial\sigma$ is stable with $\delta E > 0$ for all linear perturbation η.

If $a_0 > b_0$, the case in which the density in σ exceeds that of the exterior, the effects of density stratification and magnetic curvature reverse their roles. The magnetic curvature force is everywhere destabilizing along $\partial\sigma$. The upper half of $\partial\sigma$ is Rayleigh-Taylor stable but not sufficiently so as to override the destabilising magnetic curvature force. On the lower half of $\partial\sigma$, both density stratification and magnetic curvature are destabilizing. Hence, the boundary $\partial\sigma$ is unstable.

4. SUMMARY AND CONCLUSION

The magnetostatic solutions presented are not intended to model coronal structures in realistic details. They are theoretical examples for illustrating physical properties in basic forms, in terms of which insights might be gained for the understanding of realistic coronal objects. Thus the explicit solutions shown in Figures 1–11 illustrate how density enhancements and depletions may form as the result of the complex interplay among the Lorentz, pressure, and gravitational forces.

The equation of force balance is highly nonlinear, and this is a major obstacle to the construction of explicit models for theoretical study. Two steps led to the rich collection of solutions in this paper. The first is to render the magnetostatic equation linear and remove undesirable physical features obtaining in the far region by localizing the current density to a region bounded by a magnetic flux surface. External to this local region is a plane-parallel at atmosphere with a potential magnetic field. This in general leads to a free boundary problem involving the bounding magnetic flux surface as an unknown of the problem. The second step circumvents this formidable problem by a self-consistent construction of both interior and exterior solutions matched across a prescribed shape of the magnetic surface. In this second step, the problem reduces to solving for a potential stream function satisfying Cauchy-type boundary conditions. This is a well-known ill-posed boundary value problem in the sense that, although the existence and uniqueness of solution may be assured in most circumstances, the solution does not depend continuously on the Cauchy boundary data (Courant & Hilbert 1963). This property renders the Cauchy boundary value problem difficult to treat numerically because small changes due to numerical truncation necessarily imply unbounded changes in the solution obtained. It is interesting that the Cauchy boundary value problem in this paper can be solved exactly. Two methods were used. The one leading to the solution given by equation (38) is intuitively transparent. The other leading to the solution given by equations (49) and (52) is more important because it can be applied to quite general boundary value problems of this type.

The solutions we constructed separate into two classes, those associated with continuous pressures and magnetic fields at the boundary between the current-carrying region and the external potential region, and those with discontinuity in pressures and magnetic fields at this boundary. The former preserves linearity in the solutions so that the principle of linear superposition serves as a powerful tool to generate new solutions, as long as the boundary of the current-carrying region is invariant in the superposition. As Figures 1–7 show, this class of solutions exhibits a rich variety of magnetostatic configurations. In the next paper of this series, this class of solutions will be put to further use in the study of prominence support. The second class of solutions involving discontinuities in pressure and magnetic field is more restricted in variety. This is due to the fact that these discontinuities must ensure that the total pressure is continuous across the boundary of the current-carrying region. This boundary condition is quadratic in the magnetic field and severely limits the independent solutions available for linear superposition.

Although we are not able to study the linear hydromagnetic stability of our equilibrium solutions in a systematic manner—a separate undertaking in its own right (e.g., DeBryne & Hood 1989; Hood 1990; Zweibel 1981, 1982), the simple stability properties of sharp magnetic boundaries illustrate some important issues. Our result is a particular case of a general result due to Hu (1988). A high-density plasma confined by magnetic fields concave to it without shear is unstable by the interchange

mode associated with the magnetic curvature. Conversely, a curved magnetic field intruding into a high-density plasma is stable to the interchange mode. These are classical results in laboratory plasma physics. In the solar corona, the stabilizing or destabilizing influence of the magnetic curvature force interplays with the effect of density stratification. As the example in Figure 9 shows, this interplay leads to absolute stability of the sharp boundary $\partial\sigma$ in the case where σ is a low-density cavity, and instability in the case of σ being a density enhancement.

The former case is especially interesting. Along the top half of the circular boundary $\partial\sigma$, the destabilizing top-heavy stratification is completely compensated for by the stabilizing effect of the magnetic curvature force. Along the lower half of $\partial\sigma$, both stratification and magnetic curvature are stabilizing. Such a favorable interplay may underlie the observed stability of the cavity at the base of the coronal helmet.

The instability of $\partial\sigma$ in the other case rules it out as a possible model for the external boundary of a coronal density enhancement like the helmet structure. It is conceivable that a density enhancement with a shape of $\partial\sigma$ different from that in our particular solution could be stable. In such a structure, the top portion of $\partial\sigma$ would have stable stratification, with high density separated by $\partial\sigma$ from low density above. This stabilizing feature must dominate to compensate for the adverse magnetic curvature force. It would be interesting to construct an explicit example.

We cannot understand the structure of the coronal helmet without also considering the magnetic structure associated with the quiescent prominence which is often found at the base of the central cavity. This concern is taken up in the next paper of the series.

This work was performed during the sabbatical visit of one of us (J. R. H.) to the High Altitude Observatory. We thank Ellen Zweibel for helpful comments.

APPENDIX

The equations $\nabla \cdot \boldsymbol{B} = 0$ and $\nabla \times \boldsymbol{B} = 0$ for a potential field $\boldsymbol{B} = B_y\hat{y} + B_z\hat{z}$ reduce to

$$\frac{\partial B_y}{\partial y} + \frac{\partial B_z}{\partial z} = 0 , \tag{A1}$$

$$\frac{\partial B_z}{\partial y} - \frac{\partial B_y}{\partial z} = 0 , \tag{A2}$$

which are the Cauchy-Riemann relations associated with an analytic function W of complex variable $\omega = y + iz$ related to $\boldsymbol{B}$ by

$$B_y - iB_z = W(\omega) . \tag{A3}$$

This representation of potential fields found in classical texts like Lamb (1945) and Coulson (1958) has been used extensively in recent works (e.g., Priest & Raadu 1975; Hu & Low 1982; Malherbe & Priest 1983). If ϕ and A are the potential and stream functions of $\boldsymbol{B}$, we have

$$\begin{aligned} \boldsymbol{B} &= \frac{\partial A}{\partial z}\hat{y} - \frac{\partial A}{\partial y}\hat{z} \\ &= \frac{\partial \phi}{\partial y}\hat{y} + \frac{\partial \phi}{\partial z}\hat{z} . \end{aligned} \tag{A4}$$

Equating the components, we obtain the Cauchy-Riemann relations

$$\begin{aligned} \frac{\partial \phi}{\partial y} &= \frac{\partial A}{\partial z} , \\ \frac{\partial \phi}{\partial z} &= -\frac{\partial A}{\partial y} , \end{aligned} \tag{A5}$$

showing that $\phi + iA$ is an analytic function of ω. Using equations (A3), (A4), and (A5), it can be shown that

$$\phi + iA = \int W(\omega)d\omega . \tag{A6}$$

Equation (53) is obtained by applying equation (A6) to the potential field $\boldsymbol{H}$ given by equations (48) and (52) in the complex plane of $\xi + i\zeta$.

REFERENCES

Bernstein, I. B., Friedman, E. A., Kruskal, M. D., & Kulsrud, R. M. 1958, Proc. R. Soc. Lon. A, 244, 17
Billings, D. E. 1966, A Guide to the Solar Corona (New York: Academic Press)
Coulson, C. A. 1958, Electricity (Edinburgh: Oliver & Boyd)
Courant, R., & Hilbert, D. 1963, Methods of Mathematical Physics, II (New York: Wiley)
DeBryne, P., & Hood, A. W. 1989, Solar Phys., 123, 241
Dennis, B. R. 1985, Solar Phys., 100, 465
Dungey, J. W. 1953, MNRAS, 113, 180
Fisher, R. R. 1984, Adv. Space Res., 4, 163
Hood, A. W. 1990, Comput. Phys. Rep., 12, 177
Hu, Y. Q. 1988, ApJ, 331, 402
Hu, Y. Q., & Low, B. C. 1982, Solar Phys., 81, 107
Hundhausen, A. J. 1972, Coronal Expansion and Solar Wind (New York: Springer)
———. 1977, in Coronal Holes and High Speed Wind Streams, ed J. B. Zirker (Boulder: Colorado Assoc. Univ. Presses)
———. 1988, in Proc. 6th Internat. Solar Wind Conf., vol. 1, ed. V. Pizzo, D. G. Sime, & T. E. Holzer (NCAR TN-306)
———. 1994, in The Many Faces of the Sun: Scientific Highlights of the Solar Maximum Mission, ed. K. T. Strong, J. L. Saba, & B. M. Haisch (New York: Springer), in press
Hundhausen, J. R., Hundhausen, A. J., & Zweibel, E. G. 1981, J. Geophys. Res., 86, 11,117
Illing, R. M. E., & Hundhausen, A. J. 1986, J. Geophys. Res., 91, 10,951
Kahler, S. 1992, ARA&A, 30, 113
Lamb, H. 1945, Hydrodynamics (New York: Dover)
Low, B. C. 1975, ApJ, 197, 251
———. 1985, Solar Phys., 100, 309
Low, B. C. 1990, ARA&A, 28, 491
———. 1993, ApJ, 409, 798 (Paper L)
Low, B. C., & Hundhausen, J. R. 1994, in preparation
MacQueen, R. M. 1980, Phil. Trans. R. Soc. Lon. A, 297, 605
Malherbe, J. M., & Priest, E. R. 1983, A&A, 123, 80
Newkirk, G., Jr. 1967, ARA&A, 5, 213
Parker, E. N. 1963, Interplanetary Dynamical Processes (New York: Wiley)
———. 1979, Cosmical Magnetic Fields (Oxford: Oxford Univ. Press)
Pneuman, G. W. 1972, ApJ, 177, 793
Pneuman, G. W., & Kopp, R. A. 1971, Solar Phys., 18, 258
Poland, A. I. (ed) 1986, Coronal and Prominence Plasmas (NASA CP-2442) (Washington, DC: NASA)
Priest, E. 1982, Solar Magnetohydrodynamics (Dordrecht: Reidel)
Priest, E. R., & Raadu, M. A. 1975, Solar Phys., 43, 177
Saito, K., & Hyder, C. L. 1968, Solar Phys., 5, 61
Saito, K., & Tandberg-Hanssen, E. 1973, Solar Phys., 31, 105
Serio, S., Vaiana, G. S., Godoli, G., Motta, S., Pirronello, V., & Zappala, R. A. 1978, Solar Phys., 59, 65
Sime, D. G., & Streete, J. 1993, ApJ, 408, 368
Spitzer, L., Jr. 1967, Physics of Fully Ionized Gases (New York: Wiley)
Sturrock, P. A., & Smith, S. M. 1968, Solar Phys., 5, 87
Tandberg-Hanssen, E. 1974, Solar Prominences (Dordrecht: Reidel)
Tandberg-Hanssen, E., & Emslie, A. G. 1988, The Physics of Solar Flares (Cambridge: Cambridge Univ. Press)
Uchida, Y., & Low, B. C. 1981, J. Astrophys. Astron., 2, 405
Wu, F., & Low, B. C. 1987, ApJ, 312, 431
Zirin, H. 1988, Astrophysics of the Sun (Cambridge: Cambridge Univ. Press)
Zweibel, E. G. 1981, ApJ, 249, 731
———. 1982, ApJ, 258, L53